The EMBO Journal Vol. 21 No. 13 pp. 3454–3463, 2002

The Runx3 transcription factor regulates development and survival of TrkC dorsal root ganglia neurons

Ditsa Levanon, David Bettoun, Catherine Harris-Cerruti, Eilon Woolf, Varda Negreanu, Raya Eilam[1], Yael Bernstein, Dalia Goldenberg, Cuiying Xiao, Manfred Fliegauf[2], Eitan Kremer[3], Florian Otto[2], Ori Brenner[1], Aharon Lev-Tov[3] and Yoram Groner[4]

Departments of Molecular Genetics and [1]Veterinary Resources, The Weizmann Institute of Science, Rehovot 76100, [3]Department of Anatomy and Cell Biology, The Hebrew University Medical School, Jerusalem 91120, Israel and [2]Department of Hematology/Oncology, University of Freiburg Medical Center, D-79106 Freiburg, Germany

[4]Corresponding author
e-mail: yoram.groner@weizmann.ac.il

D.Levanon and D.Bettoun contributed equally to this work

The RUNX transcription factors are important regulators of linage-specific gene expression in major developmental pathways. Recently, we demonstrated that Runx3 is highly expressed in developing cranial and dorsal root ganglia (DRGs). Here we report that within the DRGs, *Runx3* is specifically expressed in a subset of neurons, the tyrosine kinase receptor C (TrkC) proprioceptive neurons. We show that Runx3-deficient mice develop severe limb ataxia due to disruption of monosynaptic connectivity between intraspinal afferents and motoneurons. We demonstrate that the underlying cause of the defect is a loss of DRG proprioceptive neurons, reflected by a decreased number of TrkC-, parvalbumin- and β-galactosidase-positive cells. Thus, Runx3 is a neurogenic TrkC neuron-specific transcription factor. In its absence, TrkC neurons in the DRG do not survive long enough to extend their axons toward target cells, resulting in lack of connectivity and ataxia. The data provide new genetic insights into the neurogenesis of DRGs and may help elucidate the molecular mechanisms underlying somatosensory-related ataxia in humans.

Keywords: knockout mice/Runx1-TrkA/sensory ataxia/stretch reflex arc/trigeminal ganglia

Introduction

The mammalian *RUNX3/AML2* gene, which resides on human and mouse chromosomes 1p36.1 and 4, respectively (Levanon *et al*., 1994; Avraham *et al*., 1995; Bae *et al*., 1995; Calabi *et al*., 1995), belongs to the RUNX family of transcription factors. The two other mammalian family members, RUNX1 and RUNX2, play fundamental roles in hematopoietic and osteogenic lineage-specific gene expression (Karsenty, 2000; Tracey and Speck, 2000), and when mutated are associated with human diseases (Komori and Kishimoto, 1998; Speck *et al*., 1999). RUNX3 is highly expressed in the adult hematopoietic system (Levanon *et al*., 1994, 1996; Meyers *et al*., 1996; Shi and Stavnezer, 1998; Le *et al*., 1999; Bangsow *et al*., 2001), but its biological function is largely unknown.

Members of the RUNX family share homology in a 128 amino acid region, designated runt domain (RD), first identified in the *Drosophila* pair-rule gene *runt*. The RD directs binding of RUNX proteins to DNA and mediates their interaction with the partner protein CBFβ (Ito and Bae, 1997). The three RUNX gene products have the ability to bind to the same DNA motif and to interact with common transcriptional modulators (Bruhn *et al*., 1997; Ito and Bae, 1997; Levanon *et al*., 1998; Ito, 1999). Nevertheless, they mediate distinct biological functions. These functions are orchestrated through transcriptional coupled translational control. For example, expression of Runx1 and Runx3 is regulated by two alternative promoters that exhibit distinct biological properties (Ghozi *et al*., 1996; Pozner *et al*., 2000; Bangsow *et al*., 2001). Runx1 expression is also regulated through IRES-mediated translation control (Pozner *et al*., 2000).

This fine-tuned regulation leads to a unique spatio/temporal expression pattern during development (Simeone *et al*., 1995; Komori *et al*., 1997; Otto *et al*., 1997; North *et al*., 1999; Levanon *et al*., 2001a). Sequence analysis of human and mouse genes revealed that *RUNX3/Runx3* is the smallest of the three *RUNX* genes and is, most likely, the evolutionary founder of the mammalian *RUNX* family (Bangsow *et al*., 2001).

We have previously shown that during mouse embryogenesis, Runx3 is expressed in hematopoietic organs, epidermal appendages and developing bones, as well as in sensory ganglia (Levanon *et al*., 2001a). Expression is first detected at embryonic day (E) 10.5 in both cranial and dorsal root ganglia (DRGs) (Levanon *et al*., 2001a). These findings raised the possibility that Runx3 plays a role in DRG neurogenesis.

We report here that mice functionally deficient for Runx3 exhibit marked ataxia, characterized by uncoordinated gait and abnormal positioning of the legs at rest. We show that Runx3 is specifically expressed in tyrosine kinase receptor C (TrkC) sensory neurons, whose death in the DRGs of homozygous knockout (KO) mice leads to disruption of the monosynaptic stretch reflex neuronal circuit.

The data provide new genetic information about the neurogenesis of DRGs and shed light on the largely

unknown molecular mechanisms underlying somatosensory-related ataxia in humans (Hutt and Horak, 1996).

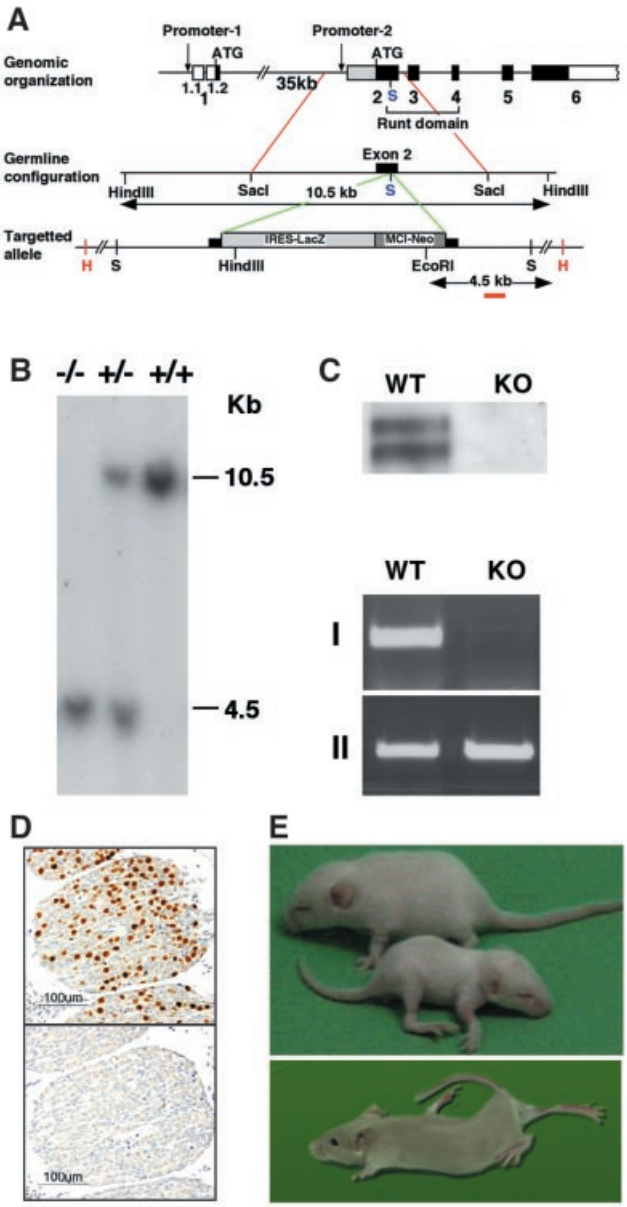

Fig. 1. Generation and phenotype of *Runx3* mutant mice. (**A**) A schematic diagram of the *Runx3* genomic locus and *Runx3*-mutant allele. The *Sac*I site used for insertion of the cassette is marked in blue. (**B**) Southern blot analysis of *Eco*RI–*Hin*dIII digest of genomic DNA isolated from tail biopsies. The 3′ external probe used here is marked in red. Wild type (+/+) shows the expected 10.5 kb band. Heterozygotes (+/–) and homozygotes (–/–) show a 4.5 kb band, which results from a new *Eco*RI site in the targeting vector. PCR analysis, using primers from *Neo* and exon 2, was employed for confirmation and rapid genotyping (not shown). (**C**) Western blot analysis (top) and RT–PCR (bottom) of proteins and RNA extracted from thymus and DRG. RT–PCR: I, Runx3; II, actin. Primers used for Runx3 are 5′-GCGGAGTAGTTCTCATCATTG-3′ (exon 1) and 5′-ATGCGTATTCCCGTAGACCCG-3′ (exon 2). (**D**) Immunostaining for Runx3 in WT DRG (upper panel) and KO (lower panel) mice. (**E**) *Runx3* KO mice were smaller (lower pup) and had a clearly recognizable phenotype, characterized by severe ataxia, extensor rigidity and posture abnormalities. The photograph depicts two 3-week-old littermates (upper) and one 2-month-old KO mouse.

Results

Homozygous Runx3 KO mice exhibit severe limb ataxia

Using the human *RUNX3* cDNA probes, we cloned and sequenced the mouse *Runx3* cDNA, as well as the relevant mouse genomic regions (Levanon *et al*., 1999; DDBJ/EMBL/GenBank accession No. AF155880). *Runx3* was disrupted, as shown in Figure 1A, by inserting a *LacZ-Neo* cassette into the RD (exon 2), at a *Sac*I site corresponding to nucleotide 3237 of the mouse gene (Negreanu *et al*., 1999; DDBJ/EMBL/GenBank accession No. AF169246). Several chimeric males were generated and used to pass on the *Runx3* mutation through the germ line. F_1 heterozygotes were intercrossed, and all three genotypes were detected in F_2 litters (Figure 1B). Transmission of the mutant allele roughly followed a Mendelian inheritance pattern, indicating that mice homozygous for the *Runx3* mutant allele are viable. Mating F_1 heterozygotes with 129/Sv, ICR or MF1 mice generated *Runx3*-mutant mice, with inbred or mixed backgrounds. In mice that are homozygous for the *Runx3* mutant allele (*Runx3* KO), no native *Runx3* mRNA or protein was detected in either DRGs or the thymus (Figure 1C and D).

Although heterozygous *Runx3* mutant mice appeared phenotypically normal, the KO mice were smaller than their wild-type (WT) and heterozygous littermates (Figure 1E). In particular, *Runx3* KO mice exhibited severe limb ataxia, characterized by uncoordinated gait and abnormal positioning of the legs at rest. Frequent extensor rigidity was observed in all four limbs and led to profound lordosis (Figure 1E; see Supplementary video clip VC available at *The EMBO Journal* Online). During the first 2 weeks of life, KO mice exhibit a high rate of mortality, particularly the 129/Sv inbred mice. The outbred KO mice were significantly more viable than the inbred mice and lived longer (at least several months), even though the neurological phenotype was similar (see Note added in proof).

Runx3 is a proprioceptive/TrkC neuron-specific transcription factor

To understand the sensory–motor defect better, we first explored the expression pattern of Runx3 in DRGs. In developing DRGs, Runx3 was first detected at E10.5 in numerous neurons (Figure 2A). The number of these neurons gradually declined so that at E16.5 significantly fewer Runx3-expressing neurons were present (Figure 2B). This developmental pattern is characteristic of neurons subserving proprioception (McMahon *et al*., 1994; Phillips and Armanini, 1996; Farinas *et al*., 1998), as further demonstrated by co-expression of Runx3 with the proprioceptive markers TrkC and parvalbumin (PV) (Mu *et al*., 1993; Honda, 1995) (Figure 2). Early in development, Runx3 was co-localized with TrkC (e.g. E12.5 in Figure 2C; data not shown), and later also with PV [e.g. postnatal day zero (P0); Figure 2D; data not shown]. No co-expression of Runx3 with either the close family member Runx1 or with TrkB was detected (Figure 2E and F). Notably, Runx3 expression was not detected in other constituents of the monosynaptic stretch reflex arc, the motoneurons and muscle spindles (not shown). These

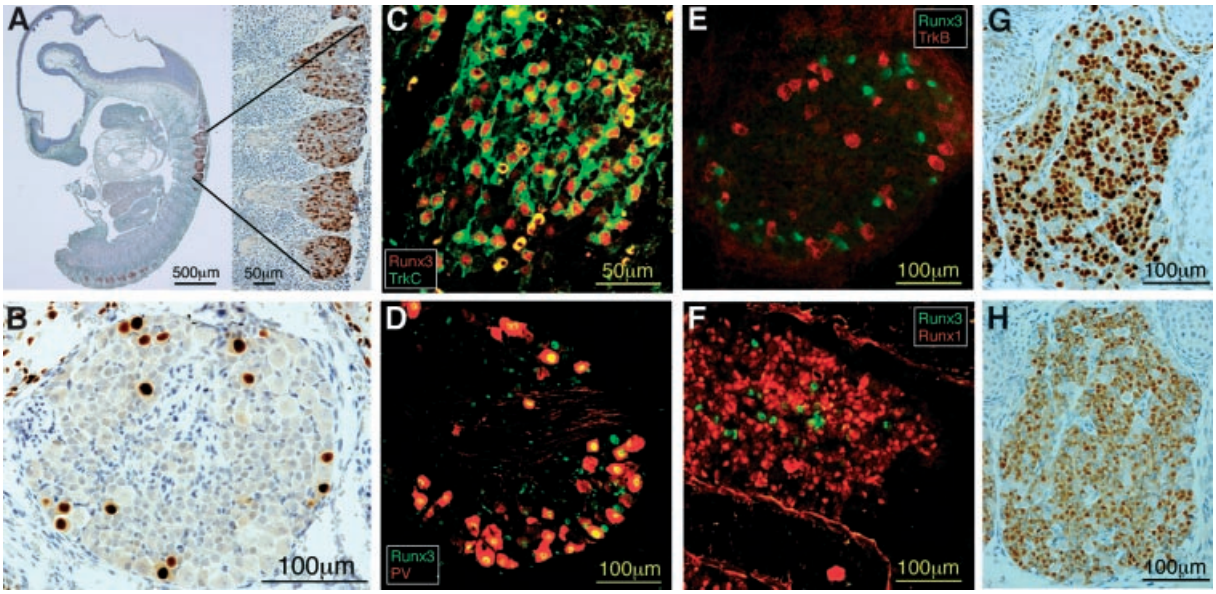

Fig. 2. Expression of Runx3 in DRG proprioceptive neurons at E10.5 (**A**) and at E16.5 (**B**). (**C**) Co-expression of Runx3 (red) and TrkC (green) at E12.5. (**D**) Co-expression of PV (red) and Runx3 (green) at P0. (**E**) Expression of Runx3 (green) and TrkB (red) in different neuronal populations (E16.5). (**F**) Expression of Runx3 (green) and Runx1 (red) in different neuronal populations (E15.5). (G and H) Typical example of Runx1 (**G**) and trkA (**H**) expression in a similar neuronal population (sections of E14.5 ganglia).

findings defined Runx3 as an early neurogenic and proprioceptive-specific transcription factor.

Of note, Runx1 expression in the DRGs started later than that of Runx3 (i.e. not seen at E10.5) and was confined to numerous small-diameter neurons, consistent with nociceptive TrkA-positive neurons. Figure 2G and H depicts a similar pattern of expression of Runx1 and TrkA, suggesting co-localization.

Lack of monosynaptic connectivity between Ia afferents and motoneurons in Runx3 KO mice

To gain insight into the physiology of the *Runx3* KO defect, we measured the synaptic transmission between dorsal root afferents and alpha motoneurons in spinal cord preparations from newborn KO and control (both WT and heterozygotes) littermate mice. Electrophysiological recordings were made in the L5 ventral root (VR) by stimulation of L5 dorsal root afferents. These electrophysiological recordings showed a short-latency monosynaptic reflex in controls, but only a small short-latency ventral root potential (VRP; arrow) in KO mice (Figure 3A). This undersized VRP was followed by a substantial long-latency polysynaptic VRP.

Simultaneous L5 VR and intracellular (IC) recordings of postsynaptic potentials (PSPs), upon graded stimulation of L5 dorsal root afferents (Figure 3B), revealed a significant short-latency PSPs in control but not in KO mice (arrow). Higher stimulation intensities elicited short-latency and time-locked reflex in controls, whereas in the KO mice a longer-latency PSP was produced. This PSP failed to induce a time-locked reflex (Figure 3B), but led to scattered motoneuron firing (Figure 3C).

The monosynaptic connectivity onto control and KO motoneurons was quantified by measuring the latency, amplitude and time to peak of the first detectable component of the PSPs (explained in Figure 3D). The results of these measurements (19 control and 23 KO motoneurons, in three and four preparations, respectively) are shown in Figure 3E. The earliest detectable PSP component in WT motoneurons is produced by activation of monosynaptic excitatory input (Lev-Tov and Pinco, 1992; Pinco and Lev-Tov, 1993; Seebach and Mendell, 1996; Li and Burke, 2001). Therefore, we used the observed latency range (4–8 ms) to classify monosynaptic excitatory postsynaptic potentials (EPSPs). Using this criterion, monosynaptic EPSPs were absent in 78% of the KO motoneurons. When EPSPs were present (in 22%), they exhibited very low amplitude (1.07 ± 0.74 mV), insufficient to elicit a monosynaptic reflex. In the majority of KO motoneurons, the first PSP component had a long latency (mean = 11.2 ± 1.8 ms) and extremely variable time to peak (between 2.6 and 22.4 ms, mean = 8.5 ± 6.6 ms), indicating the polysynaptic nature of the PSPs. Together, these data show that functional monosynaptic connectivity between Ia afferents and segmental alpha motoneurons in *Runx3* KO was completely lost.

Spinal Ia afferents are absent in Runx3 KO mice

The Ia neurons are defined by their ability to form connections with both myofibers and motoneurons. To assess the anatomical basis of the defect in synaptic connectivity, we examined the organization of intraspinal DRG projections in both control and *Runx3* KO mice. We used anterograde 1,1′-dioctadecyl-3,3,3′,3′-tetramethylindocarbocyanine perchlorate (DiI) labeling and immunostaining for PV to analyze the projections of DRG axons at P0 (Figure 4). Examination of dorsal horn laminae I–IV (Figure 4A and D) revealed heavy DiI labeling in both control and *Runx3* KO mice. However, in *Runx3* KO mice, complete loss was observed in Ia afferent projections to lamina IX of the ventral horn, where Ia afferents normally synapse with motoneurons (Figure 4B and C). The similar

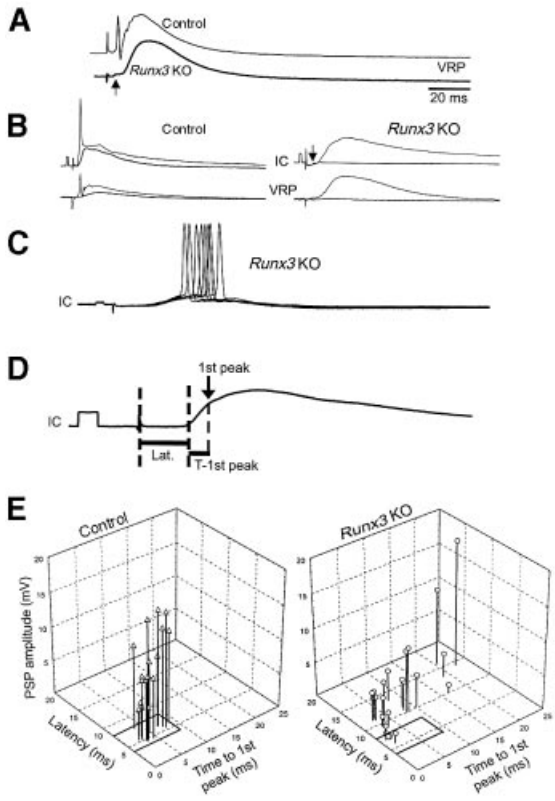

Fig. 3. Electrophysiological measurements. (**A**) Computer-averaged records (mean of 20 sweeps each) of ventral root potentials produced in the L5 segment of control and KO spinal cord by 0.1 Hz repetitive stimulation of L5 dorsal root afferents at an intensity of twice the synaptic threshold (2T). The arrow denotes a small short-latency VRP component of the *Runx3* KO VRP. (**B**) Computer-averaged records (mean of 20 sweeps each) of L5 VRPs and PSPs produced in L5 motoneurons (IC) and ventral roots (VRP) of control (left) and KO (right) mice, by 0.1 Hz stimulation of L5 dorsal root afferents at 1.1 or 2T (lower and upper trace in each pair, respectively). The arrow denotes the low-amplitude short-latency PSP component produced in the KO motoneurons. Calibration: 5 mV, 2 ms. (**C**) PSPs (eight superimposed sweeps) produced in L5 motoneurons of a KO mouse by 0.1 Hz stimulation of the L5 dorsal root afferents at 2T. Calibration: 5 mV, 2 ms. Note the scattered motoneuron firing. (**D**) Measurements of the latency (Lat.), first detectable peak (1st peak, arrow) and time to the first peak (T-1st peak) of a 20-sweep computer-averaged control PSP. Dashed lines mark the stimulus artifact, the beginning of the PSP and the occurrence of its peak. (**E**) Interrelationship between the latency, peak and time to peak of the first detectable PSP component in control and KO motoneurons. Afferent stimulation intensity (1.3–1.5T) was adjusted to obtain the maximal possible subthreshold PSP. Measurements were taken from computer-averaged records (20–40 sweeps each). One-way ANOVA followed by the modified Tukey's method for multiple comparisons $\alpha = 0.05$) was used to compare the means of each of the measured parameters of control EPSPs, *Runx3* KO EPSPs and the longer latency *Runx3* KO PSPs. These analyses revealed that the amplitude of *Runx3* KO EPSPs was much smaller than that of control EPSPs and *Runx3* KO PSPs ($p < 0.001$); that the time to peak of *Runx3* KO PSPs was significantly longer than control and *Runx3* KO EPSPs ($p < 0.05$); and that the latency of *Runx3* KO PSPs was significantly longer compared with control and *Runx3* KO EPSPs ($p < 0.001$).

DiI labeling in laminae I–IV of control and KO mice suggested that intraspinal projections of TrkA and TrkB neurons were not affected in the KO mice, consistent with the TrkC neuron specificity of Runx3.

The absence in the KO of spinal Ia afferent projections could be better appreciated by immunostaining of fibers for the proprioceptive-specific marker PV. Comparison of PV immunoreactive fibers in P0 control and *Runx3* KO mice revealed a profound loss of fibers in the spinal gray matter of the KO mice (Figure 4E and F). Of note, PV-positive fibers were also absent in spinal cord of E16.5 KO mice (not shown). DiI labeling and PV immunostaining further disclosed a difference in the territory of the dorsal gray matter between control and *Runx3* KO mice. In KO mice, the dorsal horn extended further medially than in controls (Figure 4B and C, E and F). This difference may stem from changes documented below within the white matter of the dorsal columns. These data together indicate a severe loss of proprioceptive-afferent projections in the spinal cord of the *Runx3* KO mice, consistent with the electrophysiologically documented loss of monosynaptic connectivity.

Reduced number of large-diameter axons in dorsal roots and dorsal columns of Runx3 KO mice

The central projections of DRG proprioceptive neurons reach the spinal cord via the dorsal roots. These large-diameter axons are heavily myelinated by P30 (Willis and Coggeshall, 1991). To evaluate changes in axonal size, the mean diameter of fibers was measured in cross-sections of dorsal roots of P0 and P30–P53 mice. At P0, the axons are still unmyelinated and were therefore visualized by electron microscopy. At this age, the majority of large axons in WT mice had a diameter between 1 and 1.2 μm (Figure 5AI), whereas in KO, the diameters of most axons were between 0.6 and 1 μm ($p < 0.002$), indicating a significant loss of large-diameter fibers (>1 μm). Consistent with this, the total number of myelinated axons in dorsal root was reduced by 44% in P30–P53 KO mice (WT: 2357 ± 420; KO: 1337 ± 327; two-tailed $p = 0.0143$, *t*-test) (Figure 5AII), and the cross-sectional area of the dorsal root in the KO was ~62% smaller (59 688 ± 20 892 μm^2 in controls and 23 004 ± 9208 μm^2 in KO mice; two-tailed $p < 0.024$, *t*-test).

The deficit in proprioceptive-afferent projections was also detected in the dorsal columns of KO mice. Collateral branches of proprioceptive fibers ascend to the medulla in the gracile and cuneate fascicles of the dorsal column. In P30 KO mice, the dorsal columns were narrower than in WT (Figure 4G and H), and their cross-sectional area was reduced by 39% (WT: 290 673 ± 1254 μm^2, $n = 9$; KO: 177 698 ± 793 μm^2, $n = 8$; two-tailed $p < 0.0001$, *t*-test). The KO value was corrected with consideration given to the 21% smaller size of the spinal cord. Severe depletion of large-diameter fibers was evident in this area (Figure 4I and J). Consequently, the gray matter of the dorsal horn extended bilaterally closer to the midline in KO mice. In contrast, the surface area of the cortico-spinal tract was unchanged. Taken together, these data indicate that, in the absence of Runx3, the number of large-diameter Ia fibers in dorsal roots and dorsal columns is diminished, leading to a marked reduction in the cross-sectional area of dorsal roots and dorsal columns. These results are consistent with the DiI labeling and PV immunostaining studies on the intraspinal distribution of proprioceptive projections.

Limb muscle spindles are missing in Runx3 KO mice

To assess whether in *Runx3* KO mice the peripheral Ia processes reach their peripheral target, we analyzed the

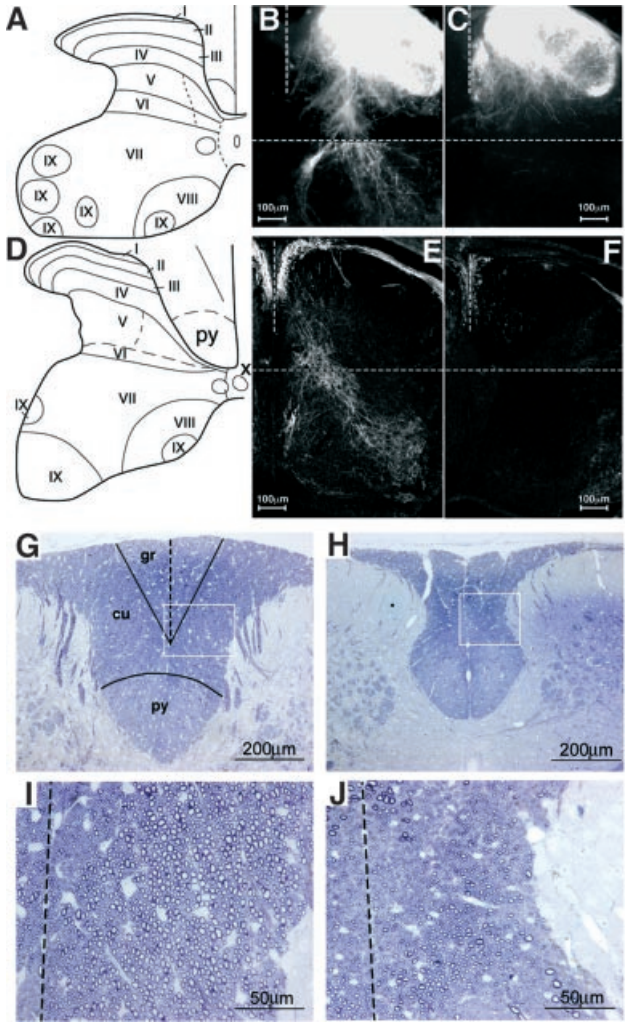

Fig. 4. Analysis of spinal cord proprioceptive afferent projections. (A and D) Schematic diagram of the spinal cord at L4 (**A**) and C6 (**D**). I–IX, cytoarchitectonic laminae. (B and C) Anterograde DiI tracing in control (**B**) and KO (**C**) mice. Transverse sections of P0 spinal cord at the L4 DRG level. (E and F) Immunostaining of PV in spinal cords of control (**E**) and KO (**F**) mice. Transverse sections at C6 DRG level at P0. (G–J) Dorsal column at high cervical level of P30 WT (**G**) and *Runx3* KO (**H**). Transverse 1 μm epon sections, stained with Toluidine Blue. gr, gracile fascicle; cu, cuneate fascicle; py, pyramidal tract. (I and J) Higher magnification of the squares in (G) and (H), showing a reduced number of large-diameter afferents in the dorsal column of KO mice (**J**) as compared with WT (**I**) (the dotted line indicates the midline).

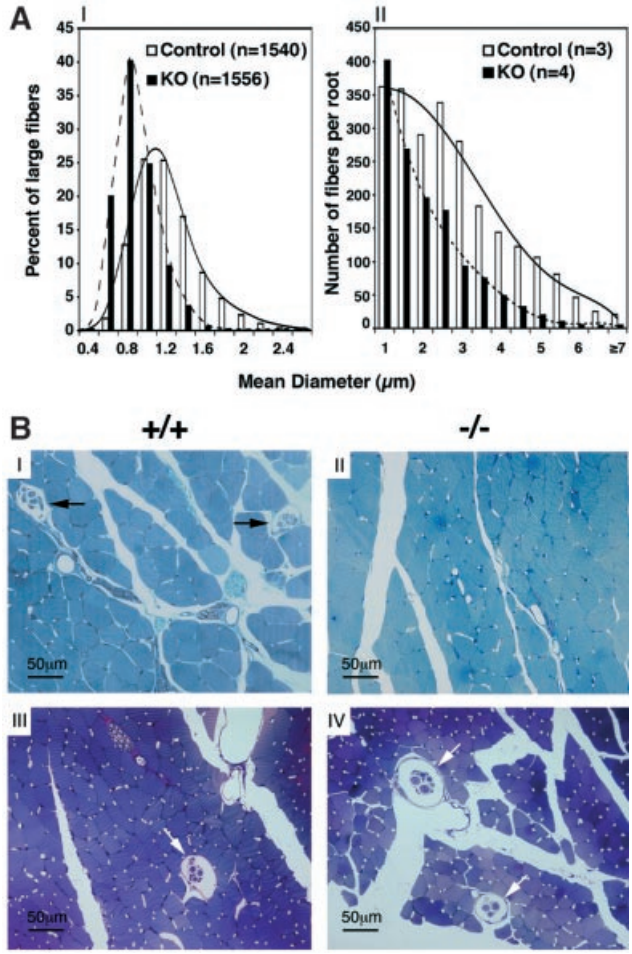

Fig. 5. (**A**) Size distribution of dorsal root fibers. Cross-sectional diameter of fibers at P0 and P30–P53. (I) Distribution of large fibers in L5 dorsal root at P0. (II) Distribution of total myelinated fibers in C7–C8 dorsal roots at P30–P53. Analysis disclosed differences between control and KO mice (Kolmogorov–Smirnov $p < 0.002$ at both ages). (**B**) Muscle spindles in limb and head muscles. Transverse thin sections of P30 soleus muscle (I and II) and P42 superficial masseter muscle (III and IV) from WT (I and III) and KO mice (II and IV) embedded in epon and stained with Toluidine Blue. Arrows indicate muscle spindles.

presence of muscle spindles in adult mice. Peripherally, the Ia sensory neurons innervate muscle spindles, which, in the mouse, are formed during E14.5–15.5 at the site of interaction between the Ia afferents and a specific subset of myotubes (Kucera *et al*., 1995). Examination in WT and KO mice of multiple appendicular muscles, such as the soleus, cranial tibial and medial gastrocnemius, revealed a complete absence of muscle spindles in KO (Figure 5BI and II). Structures representing abnormal and/or degenerate muscle spindles were not identified.

In addition to DRGs, Runx3 is expressed in cranial ganglia (Levanon *et al*., 2001a). Therefore, it was interesting to observe that, in contrast to the appendicular muscles, the number of spindles in jaw-closing muscles and other head muscles of WT and *Runx3* KO mice was apparently similar (~40 spindles in 15 serial slides with 120 μm interval taken at the level of the eyes of P42 mice; Figure 5BIII and IV). We conclude that the absence of Runx3 is associated with a distinct loss of limb muscle spindles.

Markers of proprioceptive neurons are diminished in Runx3 KO DRGs

Trk receptors are known to play a pivotal role in growth and survival of sensory neurons (Barbacid, 1994, 1995; Huang and Reichardt, 2001). We examined the effect of the absence of Runx3 on TrkC expression in DRGs and trigeminal ganglia. In agreement with previous reports (Phillips and Armanini, 1996; Farinas *et al*., 1998), TrkC expression was detected in WT mice at E10.5, early after the formation of DRGs (Figure 6AI). At this stage, a much lower level of expression was detected in KO mice, albeit fibers were clearly stained (Figure 6AII). The difference between WT and KO in the intensity of TrkC immunostaining increased during development (Figure 6AIII and

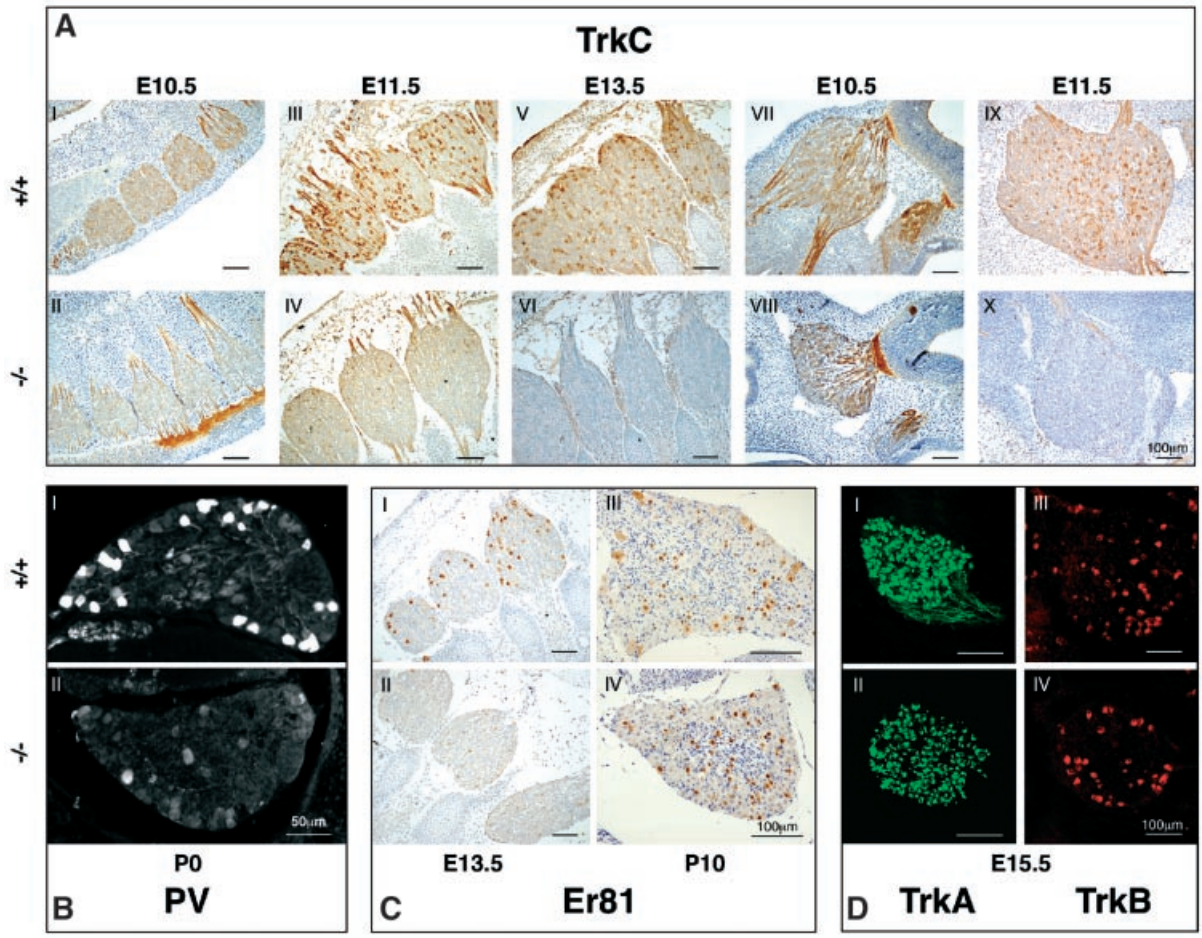

Fig. 6. Developmental pattern of proprioceptive markers in WT and *Runx3* KO mice. (**A**) Expression of TrkC in DRG (I–VI) and trigeminal ganglion (VII–X) of WT and KO mice, between E10.5 and E13.5 (E10.5, thoracic DRG; E11.5 and E13.5, cervical DRG). (**B**) Expression of PV at P0 in L5 DRG of WT (I) and KO (II) mice. Exposure of KO mice was increased 2.5 times. (**C**) Expression of Er81 in DRG of WT (I and III) and KO (II and IV) at E13.5 and P10 (E13.5, cervical; P10-L5). (**D**) Expression of TrkA and TrkB in WT (I and III) and KO (II and IV) at E15.5, cervical ganglion.

IV). By E13.5, immunostaining was completely abolished in KO cervical DRGs and fibers (Figure 6AV and VI) and was very low, compared with WT, in the sacral DRGs (not shown). In WT, Runx3 is expressed in cranial ganglia as early as E10.5 (Levanon *et al*., 2001a). We therefore examined expression of TrkC in the trigeminal ganglion. Similar to DRG, TrkC was detected in the trigeminal ganglion of KO mice at E10.5, but was absent at E11.5 (Figure 6AVII–X).

We next examined the expression of the proprioceptive-specific marker PV. As was noted above, in WT P0 mice, PV immunostaining was detected in most of the Runx3-expressing cells (Figures 2D and 6BI), whereas in the KO mice the number of PV-positive neurons was markedly decreased (Figure 6BII). The Ets transcription factor Er81 is expressed in TrkC-positive as well as in other DRG neurons (Arber *et al*., 2000). Mice lacking Er81 develop limb ataxia due to failure of group Ia proprioceptive afferents to form a discrete termination zone in the ventral spinal cord (Arber *et al*., 2000). In developing DRGs, Er81 is expressed from E13.0 (Arber *et al*., 2000) and can thus serve as an additional marker of Ia neurons. At E13.5, a marked reduction in Er81-expressing neurons was observed in *Runx3* KO, as compared with WT mice (Figure 6CI and II). At P10, on the other hand, the number of Er81-expressing cells in the KO DRGs seemed to increase, but was confined to a subpopulation of small-diameter neurons (Figure 6CIII and IV). Significantly, markers of other classes of DRG neurons, such as TrkA, TrkB and Runx1, were expressed at comparable levels in WT and *Runx3* KO mice (Figure 6DI–IV). These data indicate that, in the KO mice, the absence of Runx3 was associated with diminished expression of several proprioceptive neuron-specific markers, whereas markers of other neuronal classes remained intact.

Loss of DRG neurons in Runx3 KO mice

The diminished expression of proprioceptive markers (TrkC, PV and Er81) in the KO DRGs indicated a loss of proprioceptive neurons. Quantitative analysis of L5 DRGs in eight control and seven KO P0 mice revealed a 26% (two-tailed $p = 0.0119$, *t*-test) and 76% (two-tailed $p = 0.003$, *t*-test) reduction in the total number of neurons and in the number of large-diameter (>20 μm) neurons, respectively (Figure 7AI). Consistent with this, the volume

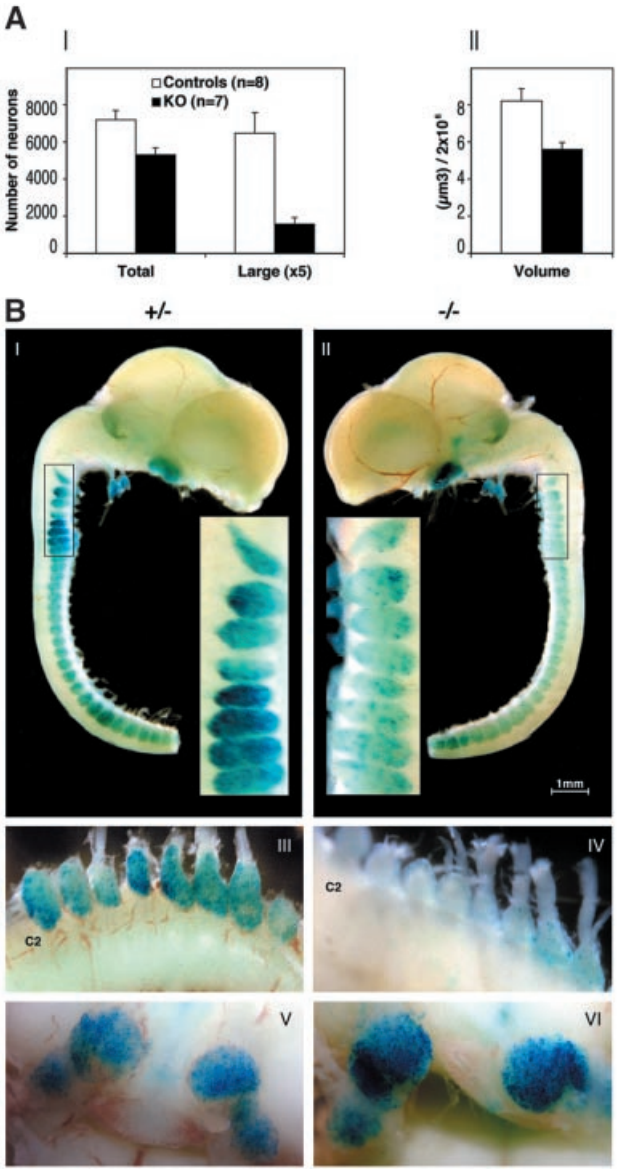

Fig. 7. Quantification of DRG neurons and analysis of β-gal activity in heterozygous and homozygous *Runx3*-mutant mice. (**A**) Neuronal count (I) and volume evaluation (II) of L5 DRG of P0 control and KO mice. Total number of neurons, number of large cells (mean diameter ⩾ 20 μm) and DRG volume (μm^3) were measured. Results are the mean of eight control (four heterozygous and four WT) and seven KO mice ± SEM. (**B**) Lateral view of dissected brain and spinal cord with attached cranial and DRG. Whole-mount E13.5 heterozygous (I) and homozygous (II) embryos stained for β-gal activity as described previously (Levanon *et al*., 2001a). (III and IV) E18.5 cervical ganglia of heterozygote (III) and KO embryo (IV). (V and VI) Ventral view showing the trigeminal ganglion bilaterally in heterozygote (V) and KO embryo (VI).

of KO DRGs was 32% (two-tailed $p = 0.0057$, *t*-test) smaller than that of control DRGs (Figure 7AII).

To follow the survival of Runx3-expressing neurons in KO mice, we analyzed expression of the *Runx3-LacZ* allele. Throughout embryonic development, the number of Runx3-positive DRG proprioceptive neurons, as monitored by X-gal staining, was much lower in homozygous KO mice than in heterozygotes. Beginning with E12.5, the earliest time detected, a marked reduction in LacZ expression was noticed in KO DRGs. The variance between heterozygotes and homozygotes was highly significant at E13.5 (Figure 7BI and II), and by E18.5 only a few X-gal-positive neurons were present in the cervical and lumbar homozygous DRGs (Figure 7BIII and IV; data not shown). Of note, the residual X-gal-positive neurons seen in sacral DRGs of E13.5 KO mice (Figure 7BII) were lost at E18.5 (data not shown), consistent with the rostro-caudal pattern of development. Conversely, in the trigeminal ganglion of homozygotes, the intensity of X-gal staining was maintained, and even increased, due to homozygosity of the LacZ allele (Figure 7BV and VI). Taken together, these data show that lack of Runx3 leads to a loss of DRG proprioceptive neurons, reflected by a reduced number of neurons and diminished X-gal-positive cells. On the other hand, TrkC neurons in trigeminal ganglia of the KO survived.

Discussion

In these studies, we demonstrate that Runx3 plays an essential role in the development and survival of DRG proprioceptive neurons; in the absence of Runx3, the sensory elements of the stretch reflex arc are disrupted, resulting in severe ataxia. The data provide a strong indication that a marked loss of proprioceptive neurons occurred in the KO DRGs, demonstrated by the complete loss of functional monosynaptic connectivity between dorsal root afferents and segmental alpha motoneurons, the absence of intraspinal Ia afferent projections, the reduced number of large-diameter Ia fibers in the dorsal roots and columns, and the lack of muscle spindles that require Ia afferents for assembly. The reduced number of DRG neurons in the KO, the lower volume of KO DRGs, and the loss of TrkC-, PV- and β-galactosidase (gal)-positive neurons further support this conclusion. Runx3 protein in DRGs was first detected at E10.5, at a stage when low levels of TrkC were still detected in KO DRGs. Thus, the most logical explanation for the above findings is that, in the absence of Runx3, Ia neurons are generated, but do not survive long enough to extend their axons toward target cells, leading to lack of synaptic connectivity and ataxia.

Among the various constituents of the stretch reflex arc, Runx3 expression is confined to the proprioceptive TrkC neurons, providing the first example of a neurogenic transcription factor specific to proprioceptive TrkC neurons (Anderson, 1999). Its distinct specificity and early onset of expression delineate Runx3 as a key regulator in the transcriptional cascade of proprioceptive TrkC neurogenesis. It was previously shown that the POU domain transcription factor Brn3a controls the neurogenesis of cranial and dorsal root ganglia neurons by regulating expression of the Trk receptors (McEvilly *et al*., 1996; Huang *et al*., 1999) as well as of other, yet to be identified, downstream genes (Huang *et al*., 2001). Since both *Runx3* and *Runx1* genes contain Brn3a binding sites in their 5′-upstream regions (Bangsow *et al*., 2001; Levanon *et al*., 2001b), it is tempting to speculate that Runx3 and Runx1 are downstream targets of Brn3a.

TrkC and NT-3 are essential for neurogenesis and survival of proprioceptive neurons (Barbacid, 1994, 1995; Silos-Santiago *et al*., 1995; Huang and Reichardt, 2001).

The anatomical and physiological manifestations of *Runx3* KO resemble those of TrkC-mutant mice (Barbacid, 1994; Farinas, 1999; Huang and Reichardt, 2001). This, along with the early loss of TrkC expression in DRGs and trigeminal ganglia of *Runx3* KO mice, may suggest that Runx3 is a positive regulator of TrkC expression. Runx3 may modulate *TrkC* transcription directly by binding to the RUNX/AML sites in the *TrkC* promoter (Ichaso *et al*., 1998) or indirectly through Gro/TLE-dependent repression of a negative regulator (Levanon *et al*., 1998). Other proprioceptive neuron-specific genes may require collaborations between Er81 and Runx3 for their expression (Giese *et al*., 1995; Ito, 1999; Arber *et al*., 2000; Gu *et al*., 2000).

In addition to its expression in DRGs, Runx3 is also highly expressed in trigeminal ganglia. Interestingly, however, TrkC neurons in these ganglia responded differently to lack of Runx3. Although TrkC levels were reduced in both DRGs and trigeminal ganglia of the KO mice, X-gal staining was reduced only in the KO DRGs. Such discrepancy in the response of DRG and trigeminal TrkC neurons was also noticed in *Brn-3a* KO mice (Huang *et al*., 2001). A differential effect on muscle spindles was also observed. In *Runx3* KO mice, muscle spindles are retained in head musculature, in contrast to their absence from the rest of the body. A similar finding was previously reported for *TrkC* KO mice (Matsuo *et al*., 2000). Of note, in *TrkC* KO and in *NT-3* KO mice, part of the trigeminal MesV neurons survive (Ernfors *et al*., 1994; Matsuo *et al*., 2000). This correlates with the presence of head muscle spindles in *TrkC* KO mice and may explain their survival in the absence of Runx3.

Based on sequence analysis, we previously proposed that *RUNX3/Runx3* is the evolutionary founder of the mammalian *RUNX* family (Bangsow *et al*., 2001). Similarly, *TrkC* may be considered as the ancestor of the Trk gene family (van Kesteren *et al*., 1998; Hallbook, 1999). Thus, it is interesting to note that both TrkC and Runx3 function in the development of the monosynaptic reflex arc, the simplest neuronal information-response circuit.

Materials and methods

Gene targeting

R1 ES cells (Nagy and Rossant, 1993) were transfected with a *Runx3* targeting vector made using a genomic *Runx3* clone derived from a 129/Sv library (Figure 1). The *LacZ-Neo* selection cassette (Otto *et al*., 1997) was inserted into exon 2 downstream of the ATG and was flanked by 2.8 and 1.8 kb of upstream and downstream regions, respectively. Homologous recombinants were evaluated by Southern analysis, using probes from upstream of the 5′ arm and downstream of the 3′ arm of the targeting vector (Figure 1). Targeted ES cells were used to create several chimeras that passed the mutation onto their progeny. All mice were bred and maintained in a pathogen-free facility.

Electrophysiology

Spinal cord preparations were isolated from 3- to 5-day-old mice of MF1 or ICR background (homozygotes = KO; heterozygotes and WT = control), as previously described for the neonatal rat spinal cord (Pinco and Lev-Tov, 1993; Kremer and Lev-Tov, 1997). Stimulation of afferents, IC recordings from motoneurons and suction electrode recordings from axon bundles in the respective ventral roots (VRP recordings) were performed as described in Lev-Tov and Pinco (1992) and Pinco and Lev-Tov (1993). The NMDA receptor blocker 2-amino-5-phosphonovaleric acid (AP5; 100 μM) was added to the bath to reduce both spontaneous and some of the stimulus-evoked polysynaptic activity (Pinco and Lev-Tov, 1993; Li and Burke, 2001). Under these conditions, stimulus-evoked, non-NMDA receptor-mediated polysynaptic activity was obtained by increasing the intensity of afferent stimulation (Pinco and Lev-Tov, 1993). Data acquisition and analyses were performed as described previously (Pinco and Lev-Tov, 1993; Kremer and Lev-Tov, 1997).

Immunohistochemistry, histology and morphometry

Embryos from timed pregnancies (the morning of the plug was considered as E0.5) were collected, fixed and sectioned (paraffin, 4 μm; cryostat, 12 μm; floating, 16 μm). Antibodies used included affinity-purified rabbit anti-RUNX1 (1:100), rabbit anti-RUNX3 (1:1000) (Levanon *et al*., 2001a), guinea pig anti-RUNX3 (1:1000), rabbit anti-TrkA (1:1000), chicken anti-TrkB (1:1000), goat anti-TrkC (1:250) (Farinas *et al*., 1998), rabbit anti-PV (1:5000 for DRG neurons and 1:1000 for afferents; Swant, Switzerland) and rabbit anti-Er81 (1:10 000) (Arber *et al*., 2000). Primary antibodies were used in a blocking solution containing 0.5% Triton X-100 and 3% normal serum from host species of the secondary antibody, in PBS. Biotinylated secondary antibodies and the ABC complex from the Vectastain kit (Vector Laboratories, Burlingame, CA) were used for detection. Alternatively, fluorophore-conjugated secondary antibodies were used (1:200–1:400; Molecular Probes).

Image-Pro Plus 4.1 was used in morphometric analysis. For neuronal counts, serial paraffin sections were stained with Nissl and neurons containing a nucleus with nucleoli were counted in every fifth section. Numbers were corrected to avoid double counting. The number of large neurons (mean diameter ⩾ 20 μm) was similarly determined and total DRG volume was calculated from the measured cross-sectional area.

P30 and P53 C7–8 dorsal roots and C2 dorsal columns were fixed with 4% paraformaldehyde/2.5% glutaraldehyde, embedded in epon, trimmed at 1 μm, stained with Toluidine Blue and evaluated by light microscopy. P0 L5 DR were processed for electron microscopy. The mean diameter of large fibers (>0.4 μm) was measured in 30–70 fields on transverse ultrathin sections at 13 500× magnification.

Muscle spindles were examined in serial sections of epon-embedded (P30 and P53; KO = 2, WT = 2) and paraffin-embedded (P42; KO = 4, WT = 4) soleus muscle, hindlimbs at the level of the tibia (P10; KO = 2, WT = 2), transverse sections of the skull (P42; KO = 2, WT = 2) and epon-embedded superficial masseter muscle (P53; KO = 1, WT = 1).

DiI tracing

The vertebral columns of P0 pups (five homozygotes, three heterozygotes and two WT of MF1 or ICR background) were isolated and fixed in 4% paraformaldehyde in PBS. DiI (Molecular Probes) crystals were applied onto DRG at the L3, L4 and L5 levels, and preparations were kept in 4% PFA at 42°C for 7 days. Vibratome cross-sections (70 μm) of L3–L5 spinal cord were analyzed for DiI fluorescence using a microscope with a rhodamine filter.

Supplementary data

Supplementary data are available at *The EMBO Journal* Online.

Acknowledgements

The authors thank Ahuva Knyszynski, Dorit Nathan, Tamara Berkuzki, Judith Chermesh, Shoshana Grossfeled and Tali Wiesel for expert assistance, Benny Geiger, Mike Fainzilber and Menahem Segal for helpful discussions, and Benny Shilo, Ari Elson, Leo Sachs and Ze'ev Paroush for comments on the manuscript. We are grateful to Louis Reichardt and Thomas Jessell for their generous gifts of antibodies. The work was supported by grants from the Commission of the EU, the Israel Science Foundation and Shapell Family Biomedical Research Foundation at the Weizmann Institute.

References

Anderson,D.J. (1999) Lineages and transcription factors in the specification of vertebrate primary sensory neurons. *Curr. Opin. Neurobiol.*, **9**, 517–524.

Arber,S., Ladle,D.R., Lin,J.H., Frank,E. and Jessell,T.M. (2000) ETS gene *Er81* controls the formation of functional connections between group Ia sensory afferents and motor neurons. *Cell*, **101**, 485–498.

Avraham,K.B., Levanon,D., Negreanu,V., Bernstein,Y., Groner,Y.,

Copeland,N.G. and Jenkins,N.A. (1995) Mapping of the runt domain gene, *Aml2*, to the distal region of mouse chromosome 4. *Genomics*, **25**, 603–605.

Bae,S.-C., Takahashi,E.-i., Zhang,Y.W., Ogawa,E., Shigesada,K., Namba,Y., Satake,M. and Ito,Y. (1995) Cloning, mapping and expression of *PEBP2aC*, a third gene encoding the mammalian runt domain. *Gene*, **159**, 245–248.

Bangsow,C. *et al*. (2001) The RUNX3 gene—sequence, structure and regulated expression. *Gene*, **279**, 221–232.

Barbacid,M. (1994) The Trk family of neurotrophin receptors. *J. Neurobiol.*, **25**, 1386–1403.

Barbacid,M. (1995) Neurotrophic factors and their receptors. *Curr. Opin. Cell Biol.*, **7**, 148–155.

Bruhn,L., Munnerlyn,A. and Grosschedl,R. (1997) ALY, a context-dependent coactivator of LEF-1 and AML-1, is required for TCRa enhancer function. *Genes Dev.*, **11**, 640–653.

Calabi,F., Rhodes,M., Williamson,P. and Boyd,Y. (1995) Identification and chromosomal mapping of a third mouse runt-like locus. *Genomics*, **26**, 607–610.

Ernfors,P., Lee,K.-F., Kucera,J. and Jaenisch,R. (1994) Lack of neurotrophin-3 leads to deficiencies in the peripheral nervous system and loss of limb proprioceptive afferents. *Cell*, **77**, 503–512.

Farinas,I. (1999) Neurotrophin actions during the development of the peripheral nervous system. *Microsc. Res. Tech.*, **45**, 233–242.

Farinas,I., Wilkinson,G.A., Backus,C., Reichardt,L.F. and Patapoutian,A. (1998) Characterization of neurotrophin and Trk receptor functions in developing sensory ganglia: direct NT-3 activation of TrkB neurons *in vivo*. *Neuron*, **21**, 325–334.

Ghozi,M.C., Bernstein,Y., Negreanu,V., Levanon,D. and Groner,Y. (1996) Expression of the human acute myeloid leukemia gene *AML1* is regulated by two promoter regions. *Proc. Natl Acad. Sci. USA*, **93**, 1935–1940.

Giese,K., Kingsley,C., Kirshner,J.R. and Grosschedl,R. (1995) Assembly and function of a TCRa enhancer complex is dependent on LEF-1-induced DNA bending and multiple protein–protein interactions. *Genes Dev.*, **9**, 995–1008.

Gu,T.L., Goetz,T.L., Graves,B.J. and Speck,N.A. (2000) Auto-inhibition and partner proteins, core-binding factor beta (CBFβ) and Ets-1, modulate DNA binding by CBFα2 (AML1). *Mol. Cell. Biol.*, **20**, 91–103.

Hallbook,F. (1999) Evolution of the vertebrate neurotrophin and Trk receptor gene families. *Curr. Opin. Neurobiol.*, **9**, 616–621.

Honda,C.N. (1995) Differential distribution of calbindin-D28k and parvalbumin in somatic and visceral sensory neurons. *Neuroscience*, **68**, 883–892.

Huang,E.J. and Reichardt,L.F. (2001) Neurotrophins: roles in neuronal development and function. *Annu. Rev. Neurosci.*, **24**, 677–736.

Huang,E.J., Zang,K., Schmidt,A., Saulys,A., Xiang,M. and Reichardt,L.F. (1999) POU domain factor Brn-3a controls the differentiation and survival of trigeminal neurons by regulating Trk receptor expression. *Development*, **126**, 2869–2882.

Huang,E.J., Liu,W., Fritzsch,B., Bianchi,L.M., Reichardt,L.F. and Xiang,M. (2001) Brn3a is a transcriptional regulator of soma size, target field innervation and axon pathfinding of inner ear sensory neurons. *Development*, **128**, 2421–2432.

Hutt,J.G. and Horak,F.B. (1996) *Gait and Balance Disorders*. McGraw-Hill, New York, NY.

Ichaso,N., Rodriguez,R.E., Martin-Zanca,D. and Gonzalez-Sarmiento,R. (1998) Genomic characterization of the human trkC gene. *Oncogene*, **17**, 1871–1875.

Ito,Y. (1999) Molecular basis of tissue-specific gene expression mediated by the runt domain transcription factor PEBP2/CBF. *Genes Cells*, **4**, 685–696.

Ito,Y. and Bae,S.-C. (1997) The Runt domain transcription factor, PEBP2/CBF and its involvement in human leukemia. In Yaniv,M. and Ghysdael,J. (eds), *Oncogenes as Transcriptional Regulators*, Vol. 2. Birkhauser Verlag, Basel, Switzerland, pp. 107–132.

Karsenty,G. (2000) Role of Cbfa1 in osteoblast differentiation and function. *Semin. Cell Dev. Biol.*, **11**, 343–346.

Komori,T. and Kishimoto,T. (1998) Cbfa1 in bone development. *Curr. Opin. Genet. Dev.*, **8**, 494–499.

Komori,T.H. *et al*. (1997) Targeted disruption of Cbfal results in a complete lack of bone formation owing to maturational arrest of osteoblasts. *Cell*, **89**, 755–764.

Kremer,E. and Lev-Tov,A. (1997) Localization of the spinal network associated with generation of hindlimb locomotion in the neonatal rat and organization of its transverse coupling system. *J. Neurophysiol.*, **77**, 1155–1170.

Kucera,J., Fan,G., Jaenisch,R., Linnarsson,S. and Ernfors,P. (1995) Dependence of developing group Ia afferents on neurotrophin-3. *J. Comp. Neurol.*, **363**, 307–320.

Le,X., Groner,Y., Kornblau,S., Gu,Y., Hittelman,W., Levanon,D., Mehta,K., Arlinghaus,R. and Chang,K. (1999) Regulation of AML2/CBFA3 in hematopoietic cells through the retinoic acid receptor α-dependent signaling pathway. *J. Biol. Chem.*, **274**, 21651–21658.

Lev-Tov,A. and Pinco,M. (1992) *In vitro* studies of prolonged synaptic depression in the neonatal rat spinal cord. *J. Physiol.*, **447**, 149–169.

Levanon,D., Negreanu,V., Bernstein,Y., Bar-Am,I., Avivi,L. and Groner,Y. (1994) *AML1*, *AML2* and *AML3*, the human members of the runt domain gene-family: cDNA structure, expression and chromosomal localization. *Genomics*, **23**, 425–432.

Levanon,D., Bernstein,Y., Negreanu,V., Ghozi,M.C., Bar-Am,I., Aloya,R., Goldenberg,D., Lotem,J. and Groner,Y. (1996) A large variety of alternatively spliced and differentially expressed mRNAs are encoded by the human acute myeloid leukemia gene *AML1*. *DNA Cell Biol.*, **15**, 175–185.

Levanon,D., Goldstein,R.E., Bernstein,Y., Tang,H., Goldenberg,D., Stifani,S., Paroush,Z. and Groner,Y. (1998) Transcriptional repression by AML1 and LEF-1 is mediated by the TLE/Groucho corepressors. *Proc. Natl Acad. Sci. USA*, **95**, 11590–11595.

Levanon,D. *et al*. (2001a) Spatial and temporal expression pattern of Runx3 (Aml2) and Runx1 (Aml1) indicates non-redundant functions during mouse embryogenesis. *Mech. Dev.*, **109**, 413–417.

Levanon,D. *et al*. (2001b) Architecture and anatomy of the genomic locus encoding the human leukemia-associated transcription factor RUNX1/AML1. *Gene*, **262**, 23–33.

Li,Y. and Burke,R.E. (2001) Short-term synaptic depression in the neonatal mouse spinal cord: effects of calcium and temperature. *J. Neurophysiol.*, **85**, 2047–2062.

Matsuo,S., Ichikawa,H., Silos-Santiago,I., Arends,J.J., Henderson,T.A., Kiyomiya,K., Kurebe,M. and Jacquin,M.F. (2000) Proprioceptive afferents survive in the masseter muscle of trkC knockout mice. *Neuroscience*, **95**, 209–216.

McEvilly,R.J., Erkman,L., Luo,L., Sawchenko,P.E., Ryan,A.F. and Rosenfeld,M.G. (1996) Requirement for Brn-3.0 in differentiation and survival of sensory and motor neurons. *Nature*, **384**, 574–577.

McMahon,S.B., Armanini,M.P., Ling,L.H. and Phillips,H.S. (1994) Expression and coexpression of Trk receptors in subpopulations of adult primary sensory neurons projecting to identified peripheral targets. *Neuron*, **12**, 1161–1171.

Meyers,S., Lenny,N., Sun,W.-H. and Hiebert,S.W. (1996) AML-2 is a potential target for transcriptional regulation by the t(8;21) and t(12;21) fusion proteins in acute leukemia. *Oncogene*, **13**, 303–312.

Mu,X., Silos-Santiago,I., Carroll,S.L. and Snider,W.D. (1993) Neurotrophin receptor genes are expressed in distinct patterns in developing dorsal root ganglia. *J. Neurosci.*, **13**, 4029–4041.

Nagy,A. and Rossant,J. (1993) production of completely ES cell derived fetuses. In Joyner,A.L. (ed.), *Gene Targeting: A Practical Approach*. Oxford University Press, Oxford, UK, pp. 147–179.

North,T., Gu,T.-L., Stacy,T., Wang,Q., Howard,L., Binder,M., Marin-Padilla,M. and Speck,N.A. (1999) Cbfa2 is required for the formation of intra-aortic hematopoietic clusters. *Development*, **126**, 2563–2575.

Otto,F. *et al*. (1997) *Cbfa1*, a candidate gene for cleidocranial dysplasia syndrome, is essential for osteoblast differentiation and bone development. *Cell*, **89**, 765–771.

Phillips,H.S. and Armanini,M.P. (1996) Expression of the trk family of neurotrophin receptors in developing and adult dorsal root ganglion neurons. *Philos. Trans. R. Soc. Lond. B Biol. Sci.*, **351**, 413–416.

Pinco,M. and Lev-Tov,A. (1993) Synaptic excitation of alpha-motoneurons by dorsal root afferents in the neonatal rat spinal cord. *J. Neurophysiol.*, **70**, 406–417.

Pozner,A., Goldenberg,D., Negreanu,V., Le,S.-Y., Elroy-Stein,O., Levanon,D. and Groner,Y. (2000) Transcription-coupled translation control of AML1/RUNX1 is mediated by cap- and internal ribosome entry site-dependent mechanisms. *Mol. Cell. Biol.*, **20**, 2297–2307.

Seebach,B.S. and Mendell,L.M. (1996) Maturation in properties of motoneurons and their segmental input in the neonatal rat. *J. Neurophysiol.*, **76**, 3875–3885.

Shi,M.J. and Stavnezer,J. (1998) CBFα3 (AML2) is induced by TGF-β1 to bind and activate the mouse germline Ig α promoter. *J. Immunol.*, **161**, 6751–6760.

Silos-Santiago,I., Greenlund,L.J., Johnson,E.M.,Jr and Snider,W.D.

(1995) Molecular genetics of neuronal survival. *Curr. Opin. Neurobiol.*, **5**, 42–49.
Simeone,A., Daga,A. and Calabi,F. (1995) Expression of runt in the mouse embryo. *Dev. Dyn.*, **203**, 61–70.
Speck,N.A., Stacy,T., Wang,Q., North,T., Gu,T.L., Miller,J., Binder,M. and Marin-Padilla,M. (1999) Core-binding factor: a central player in hematopoiesis and leukemia. *Cancer Res.*, **59**, 1789s–1793s.
Tracey,W.D. and Speck,N.A. (2000) Potential roles for RUNX1 and its orthologs in determining hematopoietic cell fate. *Semin. Cell Dev. Biol.*, **11**, 337–342.
van Kesteren,R.E., Fainzilber,M., Hauser,G., van Minnen,J., Vreugdenhil,E., Smit,A.B., Ibanez,C.F., Geraerts,W.P. and Bulloch,A.G. (1998) Early evolutionary origin of the neurotrophin receptor family. *EMBO J.*, **17**, 2534–2542.
Willis,W.D. and Coggeshall,R.E. (1991) *Sensory Mechanisms in the Spinal Cord*. Plenum, New York, NY.

Received March 28, 2002; revised May 22, 2002; accepted May 24, 2002

Note added in proof

While this manuscript was under review, Li *et al*. (*Cell*, **109**, 113–124, 2002) reported that gastric mucosa of Runx3 null mice exhibits hyperplasia and suggested that lack of Runx3 is causally related to human gastric cancer. Although the present manuscript does not address this issue, it is worth noting that a significant number of our *Runx3* KO mice lived for several (>10) months and did not develop gastric tumors.